Physica A 387 (2008) 6452–6462

Contents lists available at ScienceDirect

Physica A

journal homepage: www.elsevier.com/locate/physa

Performance of a high-dimensional R/S method for Hurst exponent estimation

Jose Alvarez-Ramirez [*,1], Juan C. Echeverria, Eduardo Rodriguez

Division de Ciencias Basicas e Ingenieria, Universidad Autonoma Metropolitana-Iztapalapa, Apartado Postal 55-534, Mexico D.F., 09340, Mexico

ARTICLE INFO

Article history:
Received 9 May 2008
Received in revised form 20 July 2008
Available online 13 August 2008

PACS:
05.40. a
05.45.Tp
87.10. e

Keywords:
Random systems
R/S analysis
Images
Hurst exponent

ABSTRACT

An extension of the R/S method to estimate the Hurst exponent of high-dimensional fractals is proposed. The method's performance was adequate when tested with synthetic surfaces having different preset Hurst exponent values and different array sizes. The two-dimensional R/S analysis is used to analyze three images from nature and experimental data, revealing interesting scaling behavior with physical meaning.

1. Introduction

Many observable signals drawn from complex systems can be characterized with concepts and methods from fractals theory. Some records of observable quantities are in the form of ordered sequences (*e.g.*, time series) and their fractal properties are commonly studied by means of a scaling analysis of the underlying fluctuations. To this purpose, several methods have been proposed in recent decades, from the classical spectral Fourier analysis to modern methods, such as R/S analysis [1], wavelet transform module maxima (WTMM) [2] and detrended fluctuation analysis (DFA) [3]. Scaling analysis methods offer advantages and drawbacks for implementation and estimation accuracy. Fourier analysis is constrained to unbiased stationary sequences. The R/S analysis has a strong theoretical back up, its statistical limitations for scaling (Hurst) exponent estimation are well established [4], and it finds wide acceptability for application in diverse econometric fields. On the other hand, due to the simplicity in implementation, the DFA is now becoming a widely used method in physics and engineering. The WTMM method was shown to be more accurate than DFA and R/S analysis, although its implementation is complicated, particularly for data sets with limited extension. In this form, diverse modifications of the R/S analysis and the DFA method have been proposed to improve performance while maintaining an easy implementation and straightforward understanding. For instance, the detrended moving average (DMA) proposed in Ref. [5] is intended to obtain a more accurate estimate of the scaling exponent over a wide of scrutinized scales. The scaling analysis methods commented on above have found applicability in a wide variety of fields, such as the analysis of DNA sequences [3], financial markets [6], daily temperature records [7], ion channels [8], EEG physiological records [9], and many more. The attractiveness of these methods

* Corresponding author. Tel.: +52 55 58044650; fax: +52 55 58044900.
E-mail address: jjar@xanum.uam.mx (J. Alvarez-Ramirez).
[1] Also at Facultad de Ingenieria, UNAM, Mexico.

0378-4371/$ – see front matter © 2008 Elsevier B.V. All rights reserved.
doi:10.1016/j.physa.2008.08.014

relies on their model-free implementation with relatively low computational burden. In this form, useful information on long-term correlations can be obtained as a preliminary step to derive stochastic models oriented to describe the dynamics of the underlying time sequence.

The performance of the scaling analysis methods for the characterization of fractality and correlations in higher-dimensional spaces has been recently addressed. The WTMM method has shown accurate results, especially for scalar and vector fields of three-dimensional (3D) turbulence [10,11], although its limitations are again related to a complex implementation and the specification of commonly ad hoc base functions. The accuracy of the DFA method has been studied by Gu and Zhou [12], showing that an accurate Hurst exponent estimation for fractal and multifractal objects (*e.g.*, images) can be obtained via a suitable selection of the detrending function. An extension of the DMA method has also been proposed [13], yielding a computationally efficient and simple procedure for the Hurst exponent estimation of synthetic and real images. The 2D height–height correlation function has also been explored to describe the scaling properties of fractured materials [14]. The existence of anomalous scaling exponents in natural images has been explored by Frenkel et al. [15] by means of Fourier principal components. The above results reveal that the analysis of natural and man-made images is of practical interest from both practical and scientific standpoints.

The performance of a high-dimensional R/S analysis that retains an easy implementation and offers a simple understanding of results is studied in this work. The method is tested using synthetic surfaces with known fractal and multifractal properties, and the numerical results are in good agreement with the corresponding DFA [12] and DMA [13] high-dimensional versions. The 2D version of the R/S method is also used to analyze three images from nature and experimental data, revealing interesting scaling behavior that is interpreted from physical grounds.

2. A high-dimensional R/S method

For convenience, a brief description of the one-dimensional R/S analysis is given as follows [1,16]. The R/S statistics is the range of partial sums of deviations of sequences from its mean, rescaled by its standard deviation. So, for a given N-dimensional vector $X_N = (x_i)$ consider an M-dimensional sample sub-vector $Y_M = (y_i)$, where $M = sN$, and $s \in (0, 1)$. Then, the R/S statistics is estimated by computing the sub-sample mean $\bar{y}_s = \frac{1}{M}\sum_{k=1}^{M} y_k$, the sequence from partial summations $z_i = \sum_{k=1}^{i} (y_k - \bar{y}_s)$, the range $R_s = \max\{z_i\} - \min\{z_i\}$, and the rescaled range $(R/S)_s = R_s/\sigma_s$, where the sample standard deviation is given by

$$\sigma_s = \left[\frac{1}{M}\sum_{k=1}^{M}(y_k - \bar{y}_s)^2\right]^{1/2}. \tag{1}$$

These steps can be summarized in the following equation [17]:

$$(R/S)_s = \frac{1}{\sigma_s}\left[\max_{1\le i\le M}\sum_{k=1}^{i}(y_k - \bar{y}_s) - \min_{1\le i\le M}\sum_{k=1}^{i}(y_k - \bar{y}_s)\right]. \tag{2}$$

The value $(R/S)_s$ corresponds to the maximum possible distance that a walker can travel with the sequence of steps Y_M. The rescaled range is estimated over a sufficiently large number of sub-vectors Y_M with different sizes s (*i.e.*, "scales") and then averaged over a sufficiently large number of sample sub-vectors over the whole fractal domain N. If the stochastic process associated to the sequence X_N is scaling over a certain domain $s \in (s_{\min}, s_{\max})$, the R/S statistics follow a power-law

$$(R/S)_s = as^H \tag{3}$$

where a is a constant and H is the Hurst scaling exponent, which is a fractal measurement of the sequence correlations. A log–log plot of $(R/S)_s$ as a function of the scale $s \in (s_{\min}, s_{\max})$ gives a straight line with slope H, which is the R/S statistics estimate of the Hurst exponent. The R/S analysis can be easily extended for multifractality estimation if the q-norm

$$\sigma_{s,q} = \left[\frac{1}{M}\sum_{k=1}^{M}(y_k - \bar{y}_s)^q\right]^{1/q} \tag{4}$$

is used instead of the standard deviation σ_s. As above, it is expected that the corresponding R/S statistics follow a power-law behavior of the form

$$(R/S)_{s,q} = a_q s^{Hq} \tag{5}$$

where H_q is the qth scaling exponent. Large values of q magnify the large fluctuations $y_i - \bar{y}_s$ from the mean $\bar{y}_s$. On the other hand, values $q \to 0$ yield a balanced weighting of large and small deviations from the mean. If H_q is constant for all $q \in \mathbb{R}$, the sequence is monofractal, meaning that the corresponding sequence was produced by only one fractal generator. Otherwise,

one says that the sequence is multifractal and has more than one fractal generator involved and perhaps nonlinearity. Multifractal sequences are more complex than monofractal ones, since the underlying sequence is produced by many fractal generators. In case of having only short-range correlations (or no correlations at all) the detrended walk profile displays properties of a standard random walk (*e.g.*, white noise) with $H_q = 0.5$. On the other hand, if $H_q < 0.5$ the correlations in the signal are *anti-persistent* (*i.e.*, with an increment very likely to be followed by a decrement), and if $H_q > 0.5$ the correlations in the signal are *persistent* (*i.e.*, with an increment very likely to be followed by an increment, and a decrement by a decrement). The value $H_q = 1.0$ corresponds to $1/f$-noise, a flicker noise that appears commonly in nature. Interestingly, the fractal dimension of the sequence X_N is related to its Hurst exponent by means of the relationship $D_{fr} = 2 - H_2$.

The R/S statistics can be easily extended for higher dimensions along similar steps. However, as we are interested in applying the R/S analysis for images, the two-dimensional case is detailed a follows. For an $N_r \times N_c$-dimensional matrix $X_{N_r,N_c} = \{x_{i,j}\}$, where N_r and N_c are respectively the numbers of rows and columns, consider a sample $M_r \times M_c$-dimensional matrix $Y_{M_r,M_c} = \{y_{i,j}\}$, where $M_r = sN_r$ and $M_c = sN_c$ (*i.e.*, the sub-sample matrix preserves the row-to-column ratio), and s is the scale considered. The R/S statistics are given by

$$(R/S)_{s,q} = \frac{1}{\sigma_{s,q}} \left[\max_{\substack{1\le i\le M_r \\ 1\le j\le M_c}} \sum_{k=1}^{i} \sum_{l=1}^{j} \left(y_{k,l} - \bar{y}_s\right) - \min_{\substack{1\le i\le M_r \\ 1\le j\le M_c}} \sum_{k=1}^{i} \sum_{l=1}^{j} \left(y_{k,l} - \bar{y}_s\right) \right] \tag{6}$$

where the mean $\bar{y}_s = \frac{1}{M_r M_c} \sum_{k=1}^{M_r} \sum_{l=1}^{M_c} y_{k,l}$ and the q-norm

$$\sigma_{s,q} = \left(\frac{1}{M_r M_c} \sum_{i=1}^{M_r} \sum_{j=1}^{M_c} \left(y_{k,l} - \bar{y}_s\right)^q \right)^{1/q} \tag{7}$$

are used. As in the one-dimensional case, the rescaled range is estimated over a sufficiently large number of sampled sub-matrices Y_{M_r,M_c} with different scales $s \in (s_{\min}, s_{\max})$ and then averaged over the whole domain $N_r \times N_c$. Since the random walk represented by the double sum $\sum_{k=1}^{m_r} \sum_{l=1}^{m_c} \left(y_{k,l} - \bar{y}_s\right)$ is made on a two-dimensional Euclidean space, the R/S statistics follow the power-law behavior

$$(R/S)_{s,q} = a_q s^{2H_q}. \tag{8}$$

A log–log plot of $(R/S)_{s,q}$ as a function of s^2 gives a straight line with slope H_q. As in the one-dimensional case, $H_q = 0.5$ indicates the lack of correlations, $H_q > 0.5$ indicates the presence of correlations, and $H_q < 0.5$ reflects anti-correlation processes. In fact, large values of H_q indicate that the two-dimensional array X_{N_r,N_c} is less complex than non-correlated random matrices. In this case, the fractal dimension and the Hurst exponent are related by $D_{fr} = 3 - H_2$.

The proposed two-dimensional R/S algorithm is characterized by short execution time and easy implementation. To this end, the implementation specifications are the following. (i) $s_{\min} = 0.025$ and $s_{\max} = 0.5$. Finite-size effects are present for scales $s < s_{\min}$. This problem also occurs with one-dimensional fractals, resulting in the overestimation of H_q in anti-correlated signals and underestimation of the Hurst exponent in correlated sequences [18]. On the other hand, for $s > s_{\max}$ the number of sub-arrays Y_{M_r,M_c} can be so small as to stabilize the R/S statistics. (ii) To reduce potential bias due to contiguous sub-series, the sub-arrays Y_{M_r,M_c} were sampled randomly, which leads to a type of partially overlapping sub-array sampling. In principle, partial overlapping should lead to an improved Hurst exponent estimation, especially for large scales where a limited number of sampled contiguous sub-series can be drawn [19]. (iii) The number of sampled sub-arrays N_{sam} was chosen according to the relationship $N_{\text{sam}} = \left\lfloor k_{\text{sam}} \frac{\min(N_r,N_c)}{s^2} \right\rfloor$, which yields a balanced sub-array sampling for the different scales in $(s_{\min}, s_{\max})$ (*i.e.*, a larger number of sampled sub-arrays for smaller scales). Here, to avoid excessive computational burden, $k_{\text{sam}} = 0.25$ is suggested.

The feasibility of the two-dimensional R/S analysis was tested with synthetic matrices representing fractional surfaces. In this work, the MATLAB software FRACLAB 2.03 developed by INRIA (http://www.irccyn.ec-nantes.fr/hebergement/FracLab) was used to synthesize fractional surfaces with assigned Hurst exponent H_2 ranging from 0.05 to 0.9 with a step of 0.05. Three domain sizes (256×256, 1024×1024 and 2056×2056) were chosen, and for each domain size 20 surfaces were generated. Fig. 1 compares the estimated Hurst exponent H_2 with respect to the preset value $H_{2,ps}$. It can be seen that the estimated Hurst exponents are very close to the preset values in general, and that the deviation becomes larger for small-size matrices. Gu and Zhou [12] mentioned that the sensitivity of two-dimensional R/S analysis is worse compared to the two-dimensional DFA sensitivity. Although Gu and Zhou's implementation was not detailed, we think that the worst performance of the R/S analysis is due to a poor sub-matrix sampling for large scales s, and that the performance can be improved by balancing the number of samples, as we have done with the guideline $N_{\text{sam}} = \left\lfloor k_{\text{sam}} \frac{\min(N_r,N_c)}{s^2} \right\rfloor$. For the 1024×1024 domain size, Fig. 2 shows the results for two R/S analysis implementations: (a) with regular sampling by dividing the domain size into $\left\lfloor \frac{\min(N_r,N_c)}{s} \right\rfloor$ disjoint phalanx segments [12], and (b) as proposed in this work, by balancing the number of samples by

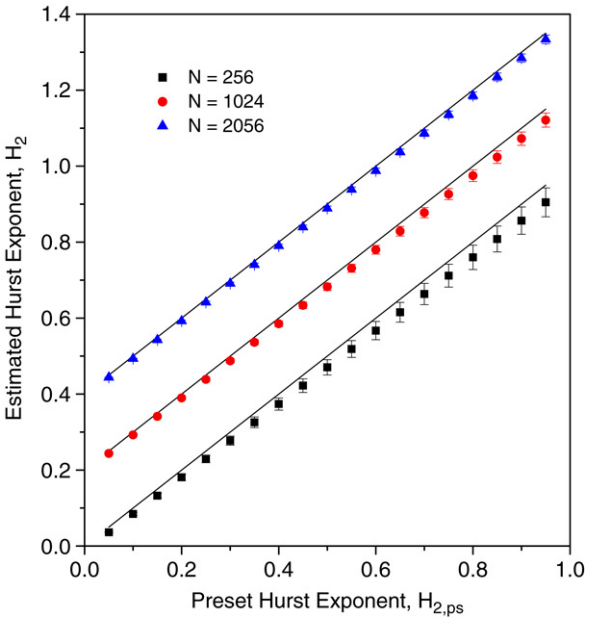

Fig. 1. Comparison of the estimated Hurst exponent H_2 with the preset value H_{pr}. The error bars show the standard deviation of the estimated values. The results corresponding to different matrix size are translated vertically for clarity.

means of random sampling and using the guideline $N_{\text{sam}} = \left[k_{\text{sam}} \frac{\min(N_r, N_c)}{s^2}\right]$. As mentioned above, the poor performance of the disjointly sampled R/S method can be due to an unbalanced sampling for large scales. For instance, for $s = 0.5$ only four sampling sub-matrices can be obtained with the regular sampling. The number of sub-matrices can be increased by considering overlapping sub-matrices, and the bias due to overlapping can be reduced by making a random sampling. This sampling scheme results in a stabilization of the R/S statistics for large scales; in turn, this allows a more robust estimation of the Hurst exponent. The above results show that the two-dimensional R/S analysis is able to capture well the self-similar nature of the fractional surfaces, resulting in precise estimation of the Hurst exponent and similar performance to the DFA [12] and moving-average low-pass filtering [13] methods.

Gu and Zhou [12] proposed a high-dimensional extension of the well-known DFA method for fractality analysis. Their results showed the acceptable performance of the DFA method over a large variety of synthetic images. The classical R/S-scaling technique removes constant trends in the original sequence and thus, theoretically, in its detrended version is equivalent to the DFA with linear fitting (denoted as DFA1). That is, the scaling exponent estimated from the R/S statistics corresponds to the scaling exponent from the DFA with linear fitting. For 256×256 and 1024×1024 image sizes, Fig. 3 presents the DFA estimation errors with linear fitting and their corresponding error bands. For comparison purposes, the R/S estimation errors are also included, and the results show that the R/S estimation error is into the error band for the DFA estimation error. In this form, these results indicate that, although the nominal DFA Hurst estimation errors are smaller than the R/S Hurst estimation errors, in practice the estimated R/S Hurst exponent cannot be rejected as a null hypothesis when compared with the DFA Hurst exponent as the accepted hypothesis. That is, the R/S method performance is statistically as good as the DFA1 method performance.

2.1. R/S analysis for anisotropy detection

The texture from a two-dimensional image is isotropic if the scaling properties are the same along any direction. For instance, the FRACLAB algorithm used to generate the synthetic images in the above analysis guarantee that the resulting images are isotropic. However, natural and man-made images can contain anisotropic features which can be detected with a two-dimensional modification of the R/S statistics described before. For a rectangular array $X_{N_r,N_c} = \{x_{i,j}\}$, let h and v denote the vertical and horizontal directions, respectively. Consider a sample $M_r \times M_c$-dimensional matrix $Y_{M_r,M_c} = \{y_{i,j}\}$, where $M_r = sN_r$ and $M_c = sN_c$ (*i.e.*, the sample matrix preserves the row-to-column ratio), and s is the scale considered. The horizontal and vertical R/S statistics are given by

$$(R/S)^h_{s,q} = \frac{1}{\sigma_{s,q}} \left[\max_{\substack{1\le i\le M_r \\ 1\le j\le M_c}} \sum_{l=1}^{j} (y_{i,l} - \bar{y}_s) - \max_{\substack{1\le i\le M_r \\ 1\le j\le M_c}} \sum_{l=1}^{j} (y_{i,l} - \bar{y}_s) \right] \tag{9}$$

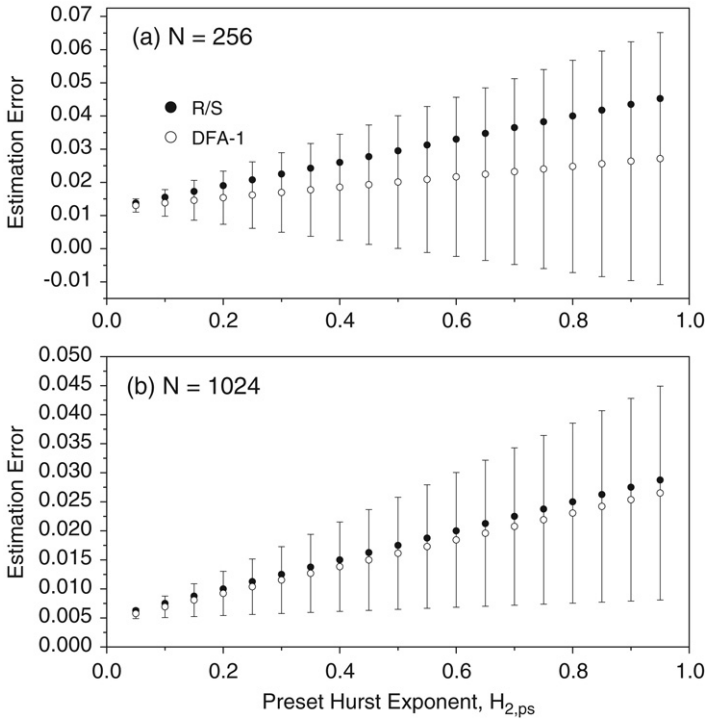

Fig. 2. Comparison of the estimated Hurst exponent H_2 with the preset value H_{pr} for regular and random (partially overlapping) samplings of a 1024×1024 domain size.

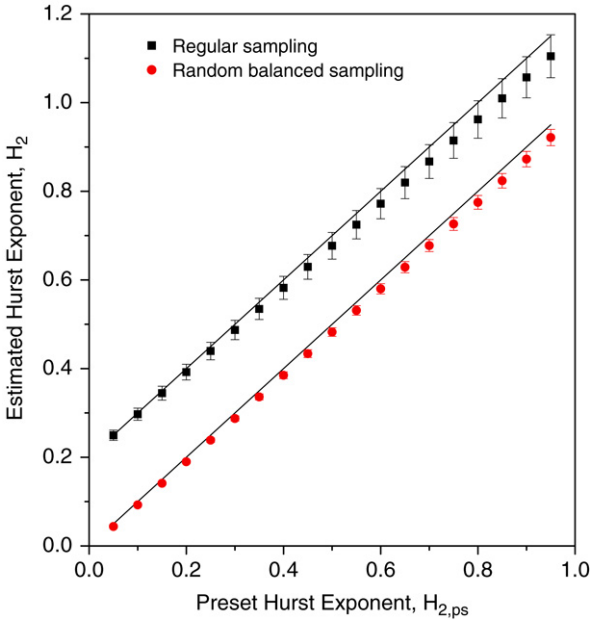

Fig. 3. Hurst estimation error and the error band 95% confidence from the DFA method with linear fitting. Also included are the Hurst estimation errors obtained from the application of the R/S statistics.

and

$$(R/S)^{v}_{s,q} = \frac{1}{\sigma_{s,q}} \left[\max_{\substack{1\le i\le M_r \\ 1\le j\le M_c}} \sum_{k=1}^{i} \left(y_{k,j} - \bar{y}_s\right) - \min_{\substack{1\le i\le M_r \\ 1\le j\le M_c}} \sum_{k=1}^{i} \left(y_{k,j} - \bar{y}_s\right) \right]. \tag{10}$$

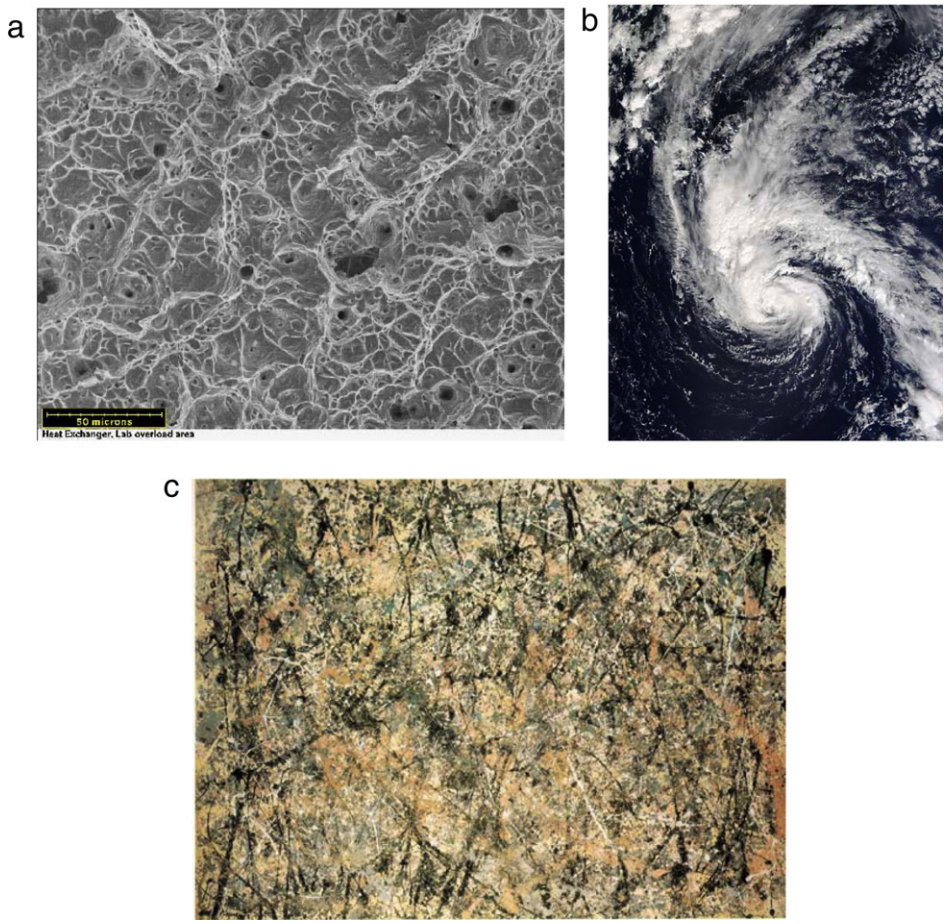

Fig. 4. Images considered for the evaluation of the two-dimensional R/S statistics. (a) SEM picture of a Series 300 stainless steel surface obtained from www.atclabs.com. (b) A 2003 Hurricane Juan image drawn from NASA's public site visibleearth.nasa.gov. (c) Jackson Pollock's drip painting Lavender Mist: Number One from www.ibiblio.org/wm/paint/auth/pollock.

Notice that in these cases the summation is carried out along only one direction, either horizontal or vertical. It is expected that the R/S statistics follow power-laws of the form

$$(R/S)^h_{s,q} = a^h_q s^{H^h_q} \tag{11}$$

and

$$(R/S)^v_{s,q} = a^v_q s^{H^v_q} \tag{12}$$

where H^h_q and H^v_q are (unidirectional) horizontal and vertical Hurst exponents, respectively. If $H^h_q \approx H^v_q$ for the scrutinized scales, one can say that the image is isotropic. On the contrary, if the differences between H^h_q and H^v_q are meaningful, the image is not isotropic as the fractality in one direction is different from the other. These ideas will be used in the following section to explore the anisotropy of diverse natural and man-made images.

3. Examples of image analysis

In this section, three real images are used to illustrate the performance of the two-dimensional R/S analysis method. The examples correspond to a typical scanning electron microscope (SEM) picture of a 300 Series stainless steel sample surface, a hurricane satellite image and a Pollock drip painting (see Fig. 4). The images, originally in any image format (*e.g.*, jpg) were converted into 256 grey level numerical matrices (level 1 for black and level 256 for white) by means of the MATLAB® signal processing toolbox, and the resulting two-dimensional matrices were used for scaling analysis via the R/S method described above. The R/S algorithm described in Section 2 was implemented as a tailored FORTRAN program and carried out within a PC machine.

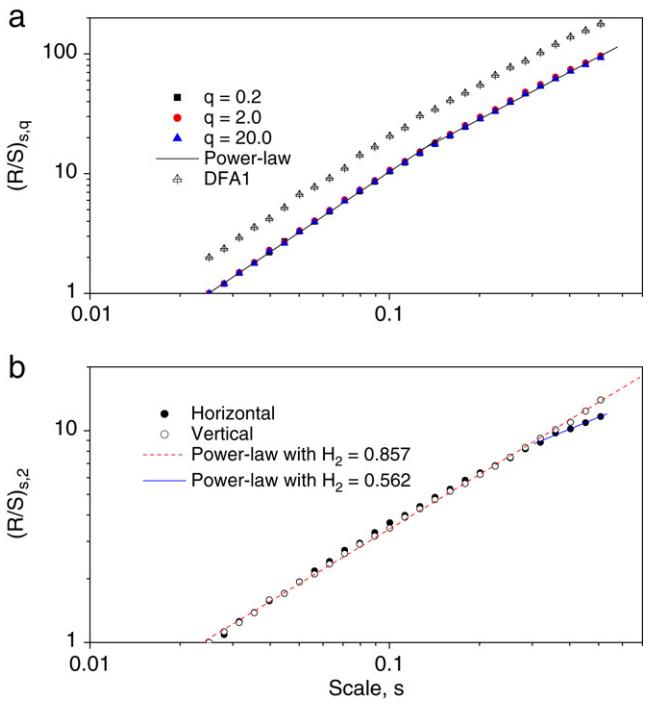

Fig. 5. (a) R/S statistics for the stainless steel SEM image shown in Fig. 4(a). Notice a crossover at about $s_{cr} = 0.14$ where the scaling behavior changes to a disordered structure for large scales. (b) Horizontal and vertical R/S statistics, showing a departure from isotropy for scales larger than about 0.31.

(a) *SEM picture*. The SEM picture is of the surface of a 300 Series stainless steel sample under mechanical overload conditions (www.atclabs.com). The size of the image is 1067 × 876 pixels. The surface, shown in Fig. 4(a), presents an irregular texture with some fractures represented by the large black islands. Fig. 5(a) illustrates the R/S statistics as a function of the scale s for different values of the norm indicator q marked with different symbols. The aggregation of the data point on a unique line indicates that the stainless steel surface image does not posses multifractal properties. On the other hand, given the presence of a crossover at about $s_{cr} = 0.14$, the data cannot be described by a unique power-law, indicating that the image self-similarity is scale-dependent. The estimated Hurst scaling exponent is $H_q = 0.841$ (± 0.0047, $p < 0.0001$) and $H_q = 0.656$ (± 0.0072, $p < 0.0001$) for $s < s_{cr}$ and $s > s_{cr}$, respectively. This shows that the stainless steel surface is less correlated for scales larger than about 28 microns. In fact, the crossover may be indicating the transition from more ordered metal grains with typical size of about 28 microns to a large-scale disordered grain array. To test the consistency of our results with respect to other methods, we have implemented the DFA1 reported by Gu and Zhou [12] with linear fitting of the fluctuations matrix (see Eq. (4) in Ref. [12]). The results are also displayed in Fig. 5(a), showing that the estimated scaling exponent is essentially the same for both methods. In fact, the deviations of the estimated Hurst exponents are not larger than ±1.5%. Fig. 5(b) presents the horizontal and vertical R/S statistics; the isotropy of the SEM picture for scales smaller than $s = 0.31$ can be appreciated. For larger scales, the horizontal Hurst exponent is close to non-correlated behavior and differs significantly from the vertical Hurst exponent. This is indicating that the stainless steel SEM image is not isotropic for large scales, and that the metal grains are arranged in a random way along the horizontal direction. That is, it is apparent that the stainless steel grains have a preferred accommodation direction.

(b) *Hurricane satellite image*. The Moderate Resolution Imaging Spectroradiometer (MODIS) on NASA's Terra satellite captured the image of Hurricane Juan (Category 5) just moments after it was declared the fifth hurricane of the season on September 26, 2003 (see Fig. 4(b)). At the time, Juan was about 160 miles east of Bermuda, and moving north at 8 miles per hour (visibleearth.nasa.gov/view_rec.php?id=5869). The hurricane image displays a typical cyclone shape with turbulent peripheral structure. The size of the image is 850 × 648 pixels. The results for the R/S statistics are shown in Fig. 6(a) for three different values of the norm indicator q. A crossover at about $s_{cr} = 0.85$ can be observed and a monofractal behavior, with estimated Hurst exponent $H_q = 0.995$ (± 0.018, $p < 0.0001$), is observed for scales smaller than $s_{cr} = 0.85$. Significant departures from the monofractal behavior are displayed for large scales, where one can observe that the Hurst exponent is larger than the one for small scales. This indicates that the large-scale image structures are more correlated than the small-scale structures, possibly reflecting the fact that the typical cyclone geometry is well-defined for scales larger than about $s = 0.1$. Fig. 6(b) shows the dependence of the large-scale Hurst exponent with the parameter q, showing that the Hurst exponent is a monotonic increasing function. This suggests that the hurricane image is multifractal for large scales and that large luminance fluctuations are more correlated (*i.e.*, more ordered) structures than small luminance fluctuations structures. This feature may reflect the fact that the strongest turbulence effect is

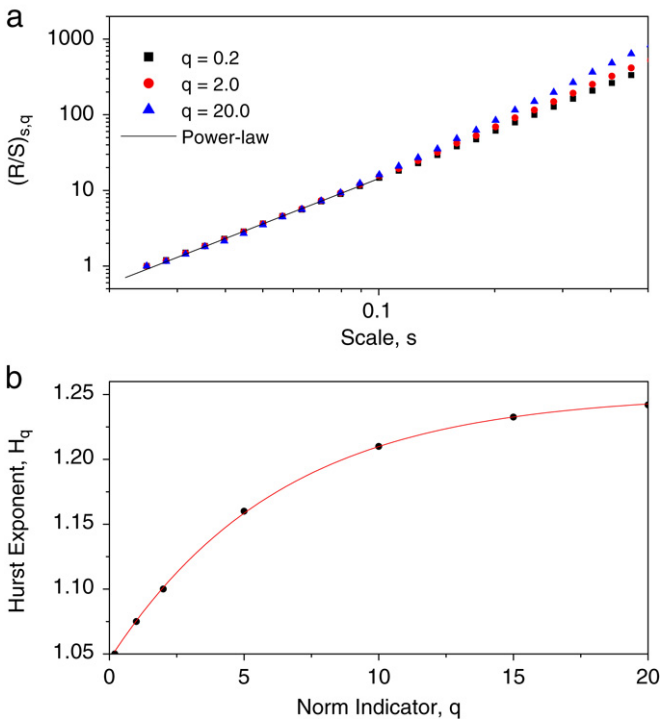

Fig. 6. Scaling analysis for the 2003 Hurricane Juan image. (a) R/S statistics showing that the image contains multifractal structures for large scales. (b) Large-scale Hurst exponent as a function of q, which shows that ordered structures are associated to the large luminance fluctuations.

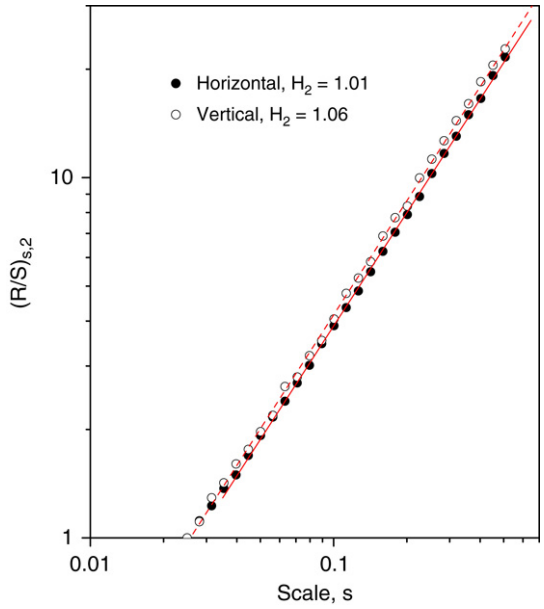

Fig. 7. Horizontal and vertical R/S statistics showing that the hurricane image is practically isotropic for all scales.

associated to the hurricane internal structure and relatively small cloud fluctuations. Fig. 7 shows the horizontal and vertical R/S statistics, showing a slight departure from isotropy over the scrutinized scales range. In fact, the vertical luminance structures are more correlated than the horizontal ones.

(c) *Pollock's drip painting*. Jackson Pollock (an abstract impressionist) was hailed as one of the greatest American painters, and was the first painter pouring paint rather than using brushes and a palette, abandoning all conventions of a central motif. Pollock danced in semi-ecstasy over canvases spread across the floor, lost in his patternings, dripping and dribbling with total control. In 1946–1950, Pollock produced a series of large-format canvas with the drip-and-

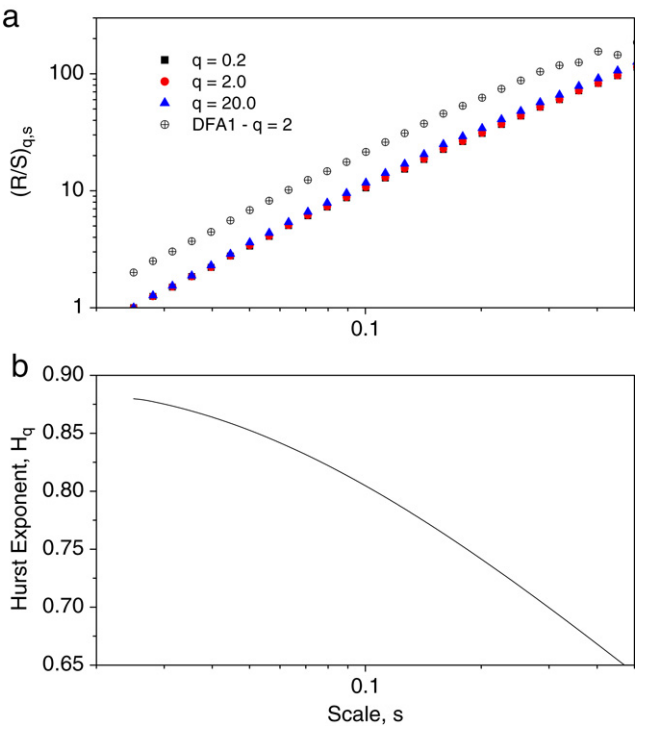

Fig. 8. Scaling analysis for the Pollock drip painting shown in Fig. 4(c). (a) R/S statistics indicating that the painting image is monofractal. (b) Hurst exponent as a function of the scale s, which shows a continuous transition towards less correlated painting structures.

pouring technique, resulting in an impressive explosion of non-figurative painting forms with a random-like structure. Under the assumption that Pollock's paintings have a fractal geometry, Taylor [20] used box-counting methods to estimate the fractal dimension of the paintings' intricate structures, obtaining that the fractal dimension increased as Pollock improved the sophistication of his painting method. In this form, Taylor concluded that Pollock used a remarkably systematic method capable of generating intricate patterns that exhibit fractal scaling criteria with precision and consistency. Here, we consider Pollock's 1950 painting Lavender Mist: Number One oil on canvas (oil, enamel, and aluminum on canvas, 221 $\times$ 300 cm at the National Gallery of Art, Washington, D.C.) shown in Fig. 4(c), to study the internal correlations by means of the two-dimensional R/S statistics. The digital 1110×814 pixels image were extracted from the internet site www.ibiblio.org/wm/paint/auth/pollock and transformed into a gray-scale numerical matrix by means of the signal processing toolbox from MATLAB®. Fig. 8(a) illustrates the dependence of the R/S statistics as a function of the scale s for different values of q marked with different symbols, showing that image is not multifractal. The results for the DFA with linear fitting are also displayed, indicating that the results obtained with the different R/S and DFA methods are essentially the same, with deviations not larger than about 2%. In fact, the main differences are found for large scales in the order of $s \geq 0.35$. The self-similarity is scale-dependent, although the existence of a crossover is not clear. Instead, it is apparent that the R/S statistics present a continuous decaying power-law exponent, which can be considered as a local (*i.e.*, scale-dependent) Hurst scaling exponent (see Fig. 8(b)). The continuous decrement of the Hurst exponent suggests that the Pollock painting is more random at large scales, with the Hurst exponent approaching 0.6 for $s = 0.5$, and that the drip-and-pouring technique yielded a fractal structure with a continuous change towards quite unpredictable painting structures. In fact, by recalling that $D_{fr} = 3 - H_2$ [21], one has that the fractal dimension increases with the scale s, achieving values of about 2.3 for $s = 0.5$. This suggests that the fractal painting structure can produce a perceptual three-dimensional effect on a two-dimensional surface. Fig. 9 presents the horizontal and vertical R/S statistics, which show that Pollock's Lavender Mist is essentially an isotropic painting over the whole scale range. However, this is not a distinctive feature of Pollock's drip-and-pouring paintings as is also shown by Fig. 9 for Pollock's Number 8 painting (see the painting at www.allposters.com/-sp/Number-8-1949-Posters_i290395_htm). In fact, the horizontal fractal structures for scales larger than about 0.1 are less correlated than the vertical structures. The results from the R/S statistics showed that Pollock's Lavender Mist painting is essentially a monofractal structure for the whole scale range. We have investigated if some multifractality features can be detected for the horizontal and vertical directions. Fig. 10 shows the estimated Hurst exponent for the horizontal and vertical directions and different values of the norm indicator q. It is observed that the Lavender Mist painting is still monofractal for both horizontal directions. However, the Number 8 painting displays interesting multifractality properties with more correlated multifractal structures along the vertical direction. This suggests that the complexity (*i.e.*, less correlated

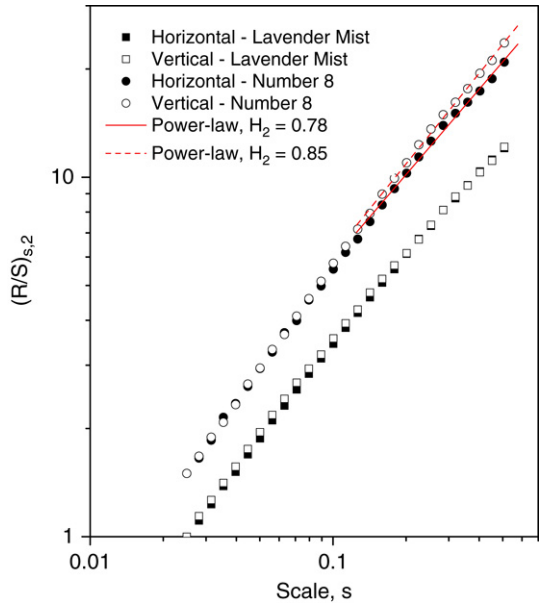

Fig. 9. Horizontal and vertical R/S statistics showing that Pollock's Lavender Mist is an isotropic painting. However, non-isotropy is obtained for a different Pollock painting (Number 8).

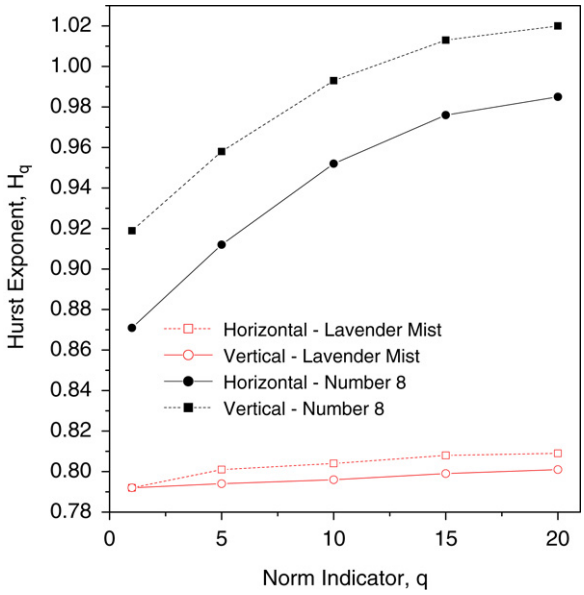

Fig. 10. Monodirectional multifractality analysis for two of Pollock's paintings. The results show a significative difference between the horizontal and vertical scaling properties for Pollock's Number 8 painting, a feature not shown by the Lavender Mist painting.

structures) in the Number 8 painting is introduced by large-scale blobs and lines arranged preferentially along the horizontal. Notice that the Hurst exponent is an increasing function of the parameter q. Since the fractal dimension and the Hurst exponent can be related by $D_{fr,q} = 3 - H_q$ [21], the results in Fig. 10 for the Number 8 painting show a fall-off of $D_{f,q}$ with q, which is in agreement with previous results on the analysis of Pollock's paintings by means of box-counting methods [22]. The differences in the scaling properties for the Lavender Mist and Number 8 paintings illustrate the ability of Pollock's drip-and-pouring technique to produce aesthetic objects with different complexity degrees. It should be stressed out that our purpose here was not to provide a detailed analysis of Pollock's paintings but to illustrate the ability of the high-dimensional R/S statistics to reveal some fractality features of Pollock's artistic work.

The above results have illustrated the ability of the R/S algorithm to provide quantitative insights into the intrinsic correlations of two-dimensional arrays. In particular, the method allows the estimation of crossovers, multifractality,

anisotropies and scale-dependent Hurst exponents. In turn, these parameters could be useful for a systematic interpretation of complex structures in other real images.

4. Conclusions

In summary, the performance of a higher-dimensional extension of the R/S analysis method was evaluated with a synthetic surface with different preset Hurst exponents and different array sizes. The results showed that the precision of the Hurst exponent estimation is improved when the array size is increased, and that larger estimation errors are found for arrays with significant correlations. The two-dimensional method was applied to the analysis of three real images from experiments, nature and art, revealing interesting scaling properties that can be interpreted to gain insights into the complex structure of the underlying fractal nature. Finally, given its ease of implementation, the R/S method can be used to investigate and characterize surface textures, landscapes, urban scenes, and many other images possessing self-similar properties. An interesting application would be the characterization the microscopic roughness of fracture surfaces [14] for materials under stress deformations. Studies in these issues should lead to automatic (noninvasive) procedures to quantify the texture of materials with different applications, from alloys to tissues.

References

[1] H.E. Hurst, Long-term storage capacity of reservoirs, Trans. Am. Soc. Civ. Eng. 116 (1951) 770.
[2] M. Holschneider, On the wavelet transformation of fractal objects, J. Stat. Phys. 50 (1988) 953.
[3] C.-K. Peng, S.V. Buldyrev, S. Havlin, M. Simons, H.E. Stanley, A.L. Goldberger, Mosaic organization of DNA nucleotides, Phys. Rev. E 49 (1994) 1685.
[4] A.W Lo, Long-term memory in stock market prices, Econometrica 59 (1991) 1279.
[5] E. Alessio, A. Carbone, G. Castelli, V. Frappietro, Second-order moving average and scaling of stochastic time series, Eur. J. Phys. B 27 (2002) 197.
[6] A. Carbone, G. Castelli, H.E. Stanley, Time-dependent Hurst exponent in financial time series, Physica A 334 (2004) 267–271.
[7] P. Talkner, R.O. Weber, Power spectrum and detrended fluctuation analysis: Application to daily temperatures, Phys. Rev. E 62 (2000) 150–160.
[8] Z. Siwy, M. Ausloos, K. Ivanova, Correlation studies of open and closed state fluctuations in an ion channel: Analysis of ion current through a large-conductance locust potassium channel, Phys. Rev. E 65 (2002) 031907.
[9] J. Lee, B. Yang, J. Lee, J. Choi, I. Choi, S. Kim, Detrended fluctuation analysis of resting EEG in depressed outpatients and healthy controls, Clinical Neurophysiology 118 (2007) 2489–2496.
[10] P. Kestener, A. Arneodo, Three-dimensional wavelet-based multifractal method: The need for revisiting the multifractal description of turbulence dissipation data, Phys. Rev. Lett. 91 (2003) 194501.
[11] P. Kestener, A. Arneodo, Generalizing the wavelet-based multifractal formalism to random vector fields: Application to three-dimensional turbulence velocity and vorticity data, Phys. Rev. Lett. 93 (2004) 044501.
[12] G.F. Gu, W.X. Zhou, Detrended fluctuation analysis for fractals and multifractals in higher dimensions, Phys. Rev. E 74 (2006) 061104.
[13] A. Carbone, Algorithm to estimate the Hurst exponent of high-dimensional fractals, Phys. Rev. E 76 (2007) 056703.
[14] L. Ponson, D. Bonamy, E. Bouchaud, Two-dimensional scaling properties of experimental fracture surfaces, Phys. Rev. Lett. 96 (2006) 035506.
[15] G. Frenkel, E. Katzav, M. Schwartz, N. Sochen, Distribution of anomalous exponents of natural images, Phys. Rev. Lett. 97 (2006) 103902.
[16] B.B. Mandelbrot, J.R. Wallis, Computer experiments with fractional noises, Water Resour. Res. 5 (1969) 228.
[17] A.W. Lo, A.C. MacKinlay, A Non-Random Walk Down Wall Street, Princeton University Press, Princeton, 1999.
[18] D.C. Caccia, D. Percival, M.J. Cannon, G. Raymond, J.B. Bassingthwaighte, Analyzing exact fractal time series: Evaluating dispersional analysis and rescaled range methods, Physica A. 246 (1997) 609.
[19] E. Craig, The sampling properties of Hurst exponent estimates, Physica A 375 (2007) 159.
[20] R.P. Taylor, A. Micolich, D. Jonas, The construction of Jackson Pollock's fractal drip paintings, Leonardo 35 (2002) 203.
[21] B.B. Mandelbrot, The Fractal Geometry of Nature Freeman, New York, 1983.
[22] J.R. Mureika, C.C. Dyer, G.C. Cupchik, Multifractal structure in nonrepresentational art, Phys. Rev. E. 72 (2005) 046101.